PERGAMON

International Journal of Solids and Structures 40 (2003) 5495–5510

INTERNATIONAL JOURNAL OF SOLIDS and STRUCTURES

www.elsevier.com/locate/ijsolstr

Elastic wave propagation in anisotropic spherical curved plates

S. Towfighi, T. Kundu *

Department of Civil Engineering and Engineering Mechanics, University of Arizona, P.O. Box 210072, Tucson, AZ 85721, USA

Received 4 March 2002; received in revised form 28 April 2003

Abstract

Spherical plate-like structures are used in pressure vessels, spherical domes of power plants, and in many other industrial applications. For non-destructive evaluation of such spherical structures, the mechanics of elastic wave propagation in spherical curved plates must be understood. The current literature shows some valuable studies on Rayleigh surface wave propagation in isotropic solids with spherical boundaries. However, the guided wave propagation problem in an anisotropic spherical curved plate, which has not been studied before, is solved for the first time in this paper.

The wave propagation, in both isotropic and anisotropic spherical curved plates, is investigated. The differential equations of motion and the stress-free boundary conditions on the inner and outer surfaces of a hollow sphere are approximately solved by a general solution technique. This solution technique was successfully utilized by the authors for solving the wave propagation problem in cylindrical plates, in their earlier works. Dispersion curves for spherical plates made of isotropic aluminum, steel, and anisotropic composite material are presented as well.

Keywords: Elastic; Propagation; Spherical

1. Introduction

Plates with spherical curvature have numerous applications in industry. While many researchers have studied the wave propagation problem in cylindrical curved plates, the spherical plates have not received due attention in the non-destructive evaluation (NDE) literature and is studied here. This study will enhance the knowledge base of the NDE community as well as the seismologists and geophysicists where anisotropy effects are significant.

Because of the importance of pipe and cylindrical pressure vessel inspections the elastic wave propagation in cylindrical structures has received a great deal of attention (Gazis, 1959a,b; Grace and Goodman, 1966; Armenkas and Reitz, 1973; Qu et al., 1996; Liu and Qu, 1998a,b; Valle et al., 1999; Towfighi et al., 2002). However, similar attention has not been given to spherical plates, even though this study is important for inspecting spherical pressure vessels, domes and earth crusts. Brekhovskikh (1968) studied the

* Corresponding author. Tel.: +1-520-621-6573; fax: +1-520-621-2550.
E-mail address: tkundu@u.arizona.edu (T. Kundu).

0020-7683/$ - see front matter © 2003 Elsevier Ltd. All rights reserved.
doi:10.1016/S0020-7683(03)00278-6

surface wave propagation in solids with curved boundary. In his study, cylindrical and spherical boundaries were considered as special cases. Lanin (1964) and Buldyrev and Lanin (1966) also investigated some aspects of wave propagation in solids with spherical boundaries. All these studies considered only one stress-free spherical boundary such as a solid sphere or a spherical void in an infinite isotropic medium. Shah et al. (1969) analyzed the three-dimensional hollow sphere using shell-theory. Gaunaurd and Werby (1991a,b) derived dispersion curves for fluid loaded spherical shells. Junger and Feit (1986), Kargl and Marston (1990), and Überal (2001) have also worked on isotropic spherical shells; however, anisotropic materials have not been considered in any of the earlier studies. The presence of 21 elastic constants in the governing differential equations requires a special solution method. This paper solves the guided wave propagation in spherical curved plates for both isotropic and anisotropic materials for the first time with a general solution technique (Towfighi, 2001). Towfighi et al. (2002) have successfully applied this technique to solve the elastic wave propagation problem in cylindrical plates.

2. Fundamental equations

The spherical coordinate system and corresponding stress and strain components are shown in Fig. 1. The equations of motion in spherical coordinates are given by

$$\begin{aligned}
&\frac{\partial\sigma_{rr}}{\partial r}+\frac{\partial\sigma_{\theta r}}{r\partial\theta}+\frac{1}{r\sin(\theta)}+\frac{\partial\sigma_{\phi r}}{\partial\phi}+\frac{2\sigma_{rr}+\cot(\theta)\sigma_{\theta r}-\sigma_{\theta\theta}-\sigma_{\phi\phi}}{r}-\rho\frac{\partial^2 u_r}{\partial t^2}=0\\
&\frac{\partial\sigma_{\theta r}}{\partial r}+\frac{\partial\sigma_{\theta\theta}}{r\partial\theta}+\frac{1}{r\sin(\theta)}\frac{\partial\sigma_{\theta\phi}}{\partial\phi}+\frac{3\sigma_{\theta r}+\cot(\theta)(\sigma_{\theta\theta}-\sigma_{\phi\phi})}{r}-\rho\frac{\partial^2 u_\theta}{\partial t^2}=0\\
&\frac{\partial\sigma_{\theta\phi}}{r\partial\theta}+\frac{\partial\sigma_{\phi r}}{\partial r}+\frac{1}{r\sin(\theta)}\frac{\partial\sigma_{\phi\phi}}{\partial\phi}+\frac{2\cot(\theta)\sigma_{\theta\phi}+3\sigma_{\phi r}}{r}-\rho\frac{\partial^2 u_\phi}{\partial t^2}=0
\end{aligned}\tag{1}$$

In the above equations, r stands for the radius in spherical coordinate system and takes values between the inner radius a and the outer radius b. θ and ϕ denote the angular quantities and directions as shown in

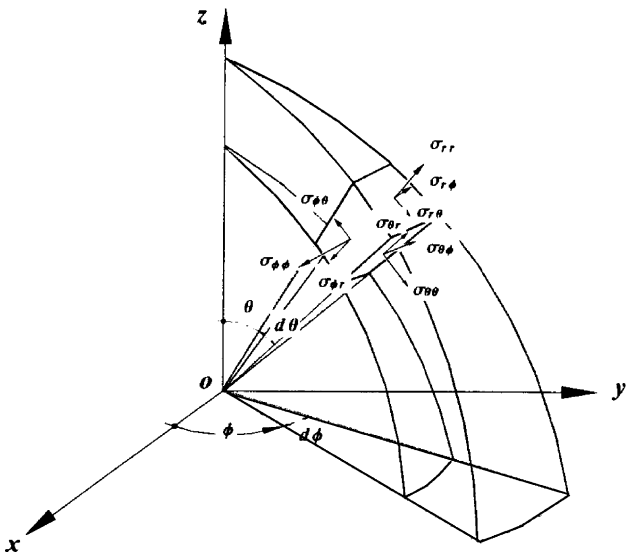

Fig. 1. Spherical coordinate system and stress components.

Fig. 1. σ and u denote stress and displacement components, respectively, and ρ indicates the mass density. For general anisotropic materials 21 elastic constants, C_{ij}, relate the stress components of Eq. (1), σ_{kl}, with the strain components, e_{kl},

$$\begin{pmatrix} \sigma_{rr} \\ \sigma_{\theta\theta} \\ \sigma_{\phi\phi} \\ \sigma_{\theta\phi} \\ \sigma_{\phi r} \\ \sigma_{\theta r} \end{pmatrix} = \begin{pmatrix} C_{11} & C_{12} & C_{13} & C_{14} & C_{15} & C_{16} \\ C_{12} & C_{22} & C_{23} & C_{24} & C_{25} & C_{26} \\ C_{13} & C_{23} & C_{33} & C_{34} & C_{35} & C_{36} \\ C_{14} & C_{24} & C_{34} & C_{44} & C_{45} & C_{46} \\ C_{15} & C_{25} & C_{35} & C_{45} & C_{55} & C_{56} \\ C_{16} & C_{26} & C_{36} & C_{46} & C_{56} & C_{66} \end{pmatrix} \cdot \begin{pmatrix} e_{rr} \\ e_{\theta\theta} \\ e_{\phi\phi} \\ 2e_{\theta\phi} \\ 2e_{\phi r} \\ 2e_{\theta r} \end{pmatrix} \tag{2}$$

The strain–displacement relations in spherical coordinates are as follows:

$$\begin{aligned} e_{rr} &= \frac{\partial u_r(r,\theta,\phi,t)}{\partial r} \\ e_{\theta\theta} &= \frac{\partial u_\theta(r,\theta,\phi,t)}{r\partial\theta} + \frac{1}{r}u_r(r,\theta,\phi,t) \\ e_{\phi\phi} &= \frac{\partial u_\phi(r,\theta,\phi,t)}{r\sin(\theta)\partial\phi} + \frac{1}{r}u_r(r,\theta,\phi,t) + \frac{1}{r}\cot(\theta)u_\theta(r,\theta,\phi,t) \\ e_{\theta\phi} &= \frac{\partial u_\theta(r,\theta,\phi,t)}{2r\sin(\theta)\partial\phi} + \frac{\partial u_\phi(r,\theta,\phi,t)}{2r\partial\theta} - \frac{1}{2r}\cot(\theta)u_\phi(r,\theta,\phi,t) \\ e_{\phi r} &= \frac{1}{2}\left(\frac{\partial u_r(r,\theta,\phi,t)}{r\sin(\theta)\partial\phi} + \frac{\partial u_\phi(r,\theta,\phi,t)}{\partial r} - \frac{u_\phi(r,\theta,\phi,t)}{r}\right) \\ e_{\theta r} &= \frac{1}{2}\left(\frac{\partial u_r(r,\theta,\phi,t)}{r\partial\theta} + \frac{\partial u_\theta(r,\theta,\phi,t)}{\partial r} - \frac{u_\theta(r,\theta,\phi,t)}{r}\right) \end{aligned} \tag{3}$$

Substitution of Eqs. (2) and (3) into Eq. (1) yields the governing differential equations in terms of displacement components. In order to eliminate the time (t) from the final governing differential equations the time dependence of the displacement components must be assumed. In the following, the waveform is postulated and then the governing differential equations are derived.

3. Waveform

In the spherical coordinate system a constant ϕ value (see Figs. 1 and 2) defines a semicircle on the surface of a sphere with radius r. All points on this semicircle rotate about the z axis as ϕ is increased continuously. The path for every point on this semicircle due to continuous increase of ϕ is a circle, and the radius of this circle is the distance between the point and the z axis, which is equal to $r\sin(\theta)$. It is assumed that the wave front on the surface of a spherical shell travels in this manner. In other words, the wave front is toroidal. The toroidal waveform has been also assumed by Kargl and Marston (1990). This waveform leads to consistent equilibrium equations. It should be noted here, that an incorrect waveform is not capable of satisfying the equations of motion and boundary conditions. Regardless of the availability of the experimental and/or numerical data for comparison, the capability of the assumed waveform to satisfy the boundary conditions and governing equations guarantees the existence of the waves, as assumed by the waveform.

When the toroidal waveform is assumed the linear phase velocity is not constant and changes with θ. In addition, the phase velocity has to be proportional to the radius of curvature to have a plane wave front in the thickness direction, see Fig. 3. Therefore, if we define c_b as the phase velocity on the outer surface of the sphere with radius b, for other points having a radius r, the phase velocity would be:

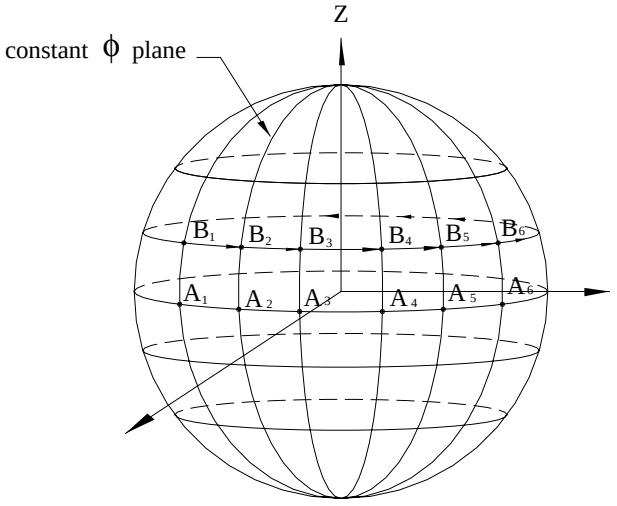

Fig. 2. Toroidal wave propagation—phase velocity is maximum at the equator, $\theta = \pi/2$.

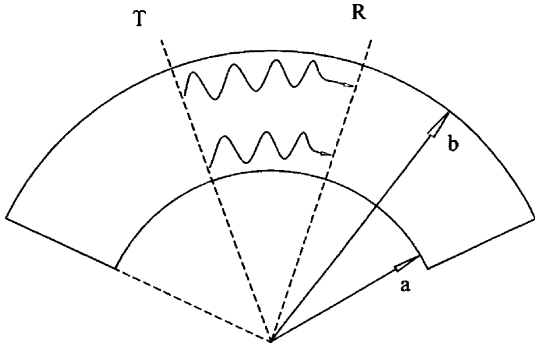

Fig. 3. Waves propagating from section T to R in a curved plate. Wave speed is proportional to the radius of curvature.

$$v_{\mathrm{ph}}(r) = c_b r/b \tag{4a}$$

For the flat plate geometry, the wave number k is defined as ω/v_{ph} because the curvature does not change. However, for a curved plate, a similar wave number expression would be r dependent. To get rid of the r dependence, the angular wave number p is defined as:

$$p = \omega/(v_{\mathrm{ph}}(r)/r) = \omega b/c_b \tag{4b}$$

The angular wave number p was initially introduced by Viktorov (1958).

For the toroidal wave travel path, as discussed above, the wave front position is a function of ϕ only because all points with the same ϕ but different θ values are in phase. Therefore, the exponential term showing the propagating wave is independent of θ. In a spherical geometry, waves travel a constant angle (ϕ) rather than a constant linear distance, in a given time interval. Note, that the linear distance varies with θ and r. This is the reason for defining the angular wave number p of Eq. (4b). The toroidal wave travel path length is defined as the product of p and ϕ. Also, note that $p\phi$ and ωt are dimensionally identical. This reasoning leads to the following waveforms.

$$
\begin{aligned}
u_r(r,\theta,\phi,t) &= U_r(r)\mathrm{e}^{\mathrm{i}p\phi-\mathrm{i}\omega t}\\
u_\theta(r,\theta,\phi,t) &= U_t(r)\mathrm{e}^{\mathrm{i}p\phi-\mathrm{i}\omega t}\\
u_\phi(r,\theta,\phi,t) &= U_f(r)\mathrm{e}^{\mathrm{i}p\phi-\mathrm{i}\omega t}
\end{aligned}
\tag{5}
$$

$U_r(r)$, $U_t(r)$ and $U_f(r)$ represent the amplitude of vibration in the radial, and two tangential directions, respectively and "i" is the imaginary number $\sqrt{-1}$.

4. Governing differential equations

Substituting the above definitions into equations of motion (1), one obtains the governing differential equations as a function of θ. The obtained equations must be satisfied for all points on the sphere where θ varies from zero to π. Note that if we substitute $\theta = \pi/2$, then the solution gives the wave propagation characteristics near the equator of the sphere. For studying wave propagation in a spherical plate segment, from point A_1 to A_2, the two points A_1 and A_2 can always be aligned along the equator of a sphere by adjusting the positions of the north and south poles. Therefore, for studying the wave propagation between two points in a spherical plate segment, it is sufficient to solve the governing equations for $\theta = \pi/2$ only. However, for studying the toroidal wave propagation in a complete sphere, the governing equations must be satisfied for all values of θ. Since, in this paper, we are only interested in the wave propagation analysis in a spherical plate segment, not the complete sphere, we simplify the problem by substituting $\theta = \pi/2$ in the governing equation. This leads to the following differential equations:

$$
\begin{aligned}
&-C_{35}U_f(r)p^2 - C_{55}U_r(r)p^2 - C_{45}U_t(r)p^2 + \mathrm{i}C_{13}U_f(r)p - \mathrm{i}C_{23}U_f(r)p - \mathrm{i}C_{33}U_f(r)p\\
&- \mathrm{i}C_{55}U_f(r)p + \mathrm{i}C_{15}U_r(r)p + \mathrm{i}C_{14}U_t(r)p - \mathrm{i}C_{24}U_t(r)p - \mathrm{i}C_{34}U_t(r)p - \mathrm{i}C_{56}U_t(r)p\\
&+ \mathrm{i}rC_{13}U_f'(r)p + \mathrm{i}rC_{55}U_f'(r)p + 2\mathrm{i}rC_{15}U_r'(r)p + \mathrm{i}rC_{14}U_t'(r)p + \mathrm{i}rC_{56}U_t'(r)p\\
&- C_{15}U_f(r) + C_{25}U_f(r) + C_{35}U_f(r) + C_{46}U_f(r) + r^2\rho\omega^2U_r(r) + C_{12}U_r(r) + C_{13}U_r(r)\\
&- C_{22}U_r(r) - 2C_{23}U_r(r) - C_{33}U_r(r) - C_{16}U_t(r) + C_{26}U_t(r) + rC_{15}U_f'(r) - rC_{25}U_f'(r)\\
&- rC_{35}U_f'(r) + 2rC_{11}U_r'(r) + rC_{16}U_t'(r) - rC_{26}U_t'(r) - rC_{36}U_t'(r) + r^2C_{15}U_f''(r)\\
&+ r^2C_{11}U_r''(r) + r^2C_{16}U_t''(r) = 0\\
&-C_{34}U_f(r)p^2 - C_{45}U_r(r)p^2 - C_{44}U_t(r)p^2 + 2\mathrm{i}C_{36}U_f(r)p - \mathrm{i}C_{45}U_f(r)p + \mathrm{i}C_{24}U_f(r)p\\
&+ \mathrm{i}C_{34}U_r(r)p + 2\mathrm{i}C_{56}U_r(r)p + \mathrm{i}C_{46}U_t(r)p + \mathrm{i}rC_{36}U_f'(r)p + \mathrm{i}rC_{45}U_f'(r)p + \mathrm{i}rC_{14}U_r'(r)p\\
&+ \mathrm{i}rC_{56}U_r'(r)p + 2\mathrm{i}rC_{46}U_t'(r)p + C_{24}U_f(r) - 2C_{56}U_f(r) + 2C_{26}U_r(r) + 2C_{36}U_r(r)\\
&+ r^2\rho\omega^2U_t(r) - C_{23}U_t(r) - 2C_{66}U_t(r) + 2rC_{56}U_f'(r) + 3rC_{16}U_r'(r) + rC_{26}U_r'(r)\\
&+ rC_{36}U_r'(r) + 2rC_{66}U_t'(r) + r^2C_{56}U_f''(r) + r^2C_{16}U_r''(r) + r^2C_{66}U_t''(r) = 0\\
&-C_{33}U_f(r)p^2 - C_{35}U_r(r)p^2 - C_{34}U_t(r)p^2 + \mathrm{i}C_{35}U_f(r)p + \mathrm{i}C_{23}U_r(r)p + \mathrm{i}C_{33}U_r(r)p\\
&+ 2\mathrm{i}C_{55}U_r(r)p - \mathrm{i}C_{36}U_t(r)p + 2\mathrm{i}C_{45}U_t(r)p + 2\mathrm{i}rC_{35}U_f'(r)p + \mathrm{i}rC_{13}U_r'(r)p\\
&+ \mathrm{i}rC_{55}U_r'(r)p + \mathrm{i}rC_{36}U_t'(r)p + \mathrm{i}rC_{45}U_t'(r)p + r^2\rho\omega^2U_f(r) + C_{44}U_f(r) - 2C_{55}U_f(r)\\
&+ 2C_{25}U_r(r) + 2C_{35}U_r(r) - C_{34}U_t(r) - 2C_{56}U_t(r) + 2rC_{55}U_f'(r) + 3rC_{15}U_r'(r) + rC_{25}U_r'(r)\\
&+ rC_{35}U_r'(r) + 2rC_{56}U_t'(r) + r^2C_{55}U_f''(r) + r^2C_{15}U_r''(r) + r^2C_{56}U_t''(r) = 0
\end{aligned}
\tag{6}
$$

In the above expressions the prime ($'$) and double prime ($''$) indicate first and second derivatives, respectively, with respect to the argument r.

5. Boundary conditions

Enforcing the stress-free boundary conditions on inner and outer surfaces the following equations are obtained for $r = a$ and b and $\theta = \pi/2$:

$$\begin{aligned}
&\mathrm{i}pC_{13}U_f(r) - C_{15}U_f(r) + C_{12}U_r(r) + C_{13}U_r(r) + \mathrm{i}pC_{15}U_r(r) + \mathrm{i}pC_{14}U_t(r)\\
&\quad - C_{16}U_t(r) + rC_{15}U'_f(r) + rC_{11}U'_r(r) + rC_{16}U'_t(r) = 0\\
&\mathrm{i}pC_{36}U_f(r) - C_{56}U_f(r) + C_{26}U_r(r) + C_{36}U_r(r) + \mathrm{i}pC_{56}U_r(r) + \mathrm{i}pC_{46}U_t(r)\\
&\quad - C_{66}U_t(r) + rC_{56}U'_f(r) + rC_{16}U'_r(r) + rC_{66}U'_t(r) = 0\\
&\mathrm{i}pC_{35}U_f(r) - C_{55}U_f(r) + C_{25}U_r(r) + C_{35}U_r(r) + \mathrm{i}pC_{55}U_r(r) + \mathrm{i}pC_{45}U_t(r)\\
&\quad - C_{56}U_t(r) + rC_{55}U'_f(r) + rC_{15}U'_r(r) + rC_{56}U'_t(r) = 0
\end{aligned} \tag{7}$$

6. Solution

It can be seen that all three differential equations are functions of three displacement components $U_r(r)$, $U_t(r)$, $U_f(r)$ and their derivatives. It should also be noted that those are functions of the radius only and appear in all equations. Therefore, three coupled differential equations and six boundary conditions must be satisfied simultaneously.

To solve the equations, the unknown functions are expanded in Fourier Series (FS). Substitution of FS expansions into the differential equations provides three algebraic equations that must be satisfied for the entire problem domain. To satisfy the equations for a given number of FS terms weighted residuals integration with a linear weight function has been carried out.

$$R = \int_a^b wf(r, x_i)\,\mathrm{d}r = 0 \tag{8}$$

Details of the above calculations are cumbersome to follow here; however, the form and dependency of functions can be reviewed. In the above expression, w is the weight function, which is equal to one for a point within the inner and outer surfaces of the plate and zero at the boundaries. The two segments of w are:

$$w_1(r, c) = \frac{r - a}{c - a} \quad w_2(r, c) = \frac{r - b}{c - b} \tag{9}$$

And $r = c$ is the radius for the peak point. It is obvious that the integration will be performed in two parts. The differential equations are a function of $U_r(r)$, $U_t(r)$, $U_f(r)$ and their derivatives, p, C_{ij}, ρ, ω and r, and can be represented in the following form:

$$f[r, U_r(r), U_t(r), U_f(r), p, \omega, \rho, C_{ij}] = 0 \tag{10}$$

The FS expansion of amplitude functions introduces new parameters x_i. For instance $U_r(r)$ must be replaced by:

$$U_r(r) = x_0 + \sum_{n=1}^{m} \left\{ \cos\left\{\frac{n\pi r}{L}\right\} x_n + \sin\left\{\frac{n\pi r}{L}\right\} x_{m+n} \right\} \tag{11}$$

Derivatives of $U_r(r)$, $U_t(r)$ and $U_f(r)$ are obtained and substituted into the differential equations with similar FS expressions. This leads to the following form for the expressions.

$$f[r, p, \omega, \rho, x_i, C_{ij}] = 0 \tag{12}$$

Note that p is independent of r. Since r is the independent variable and other arguments are constants by substituting (12) into (8) one obtains:

$$\int_a^b g[r, p, \omega, \rho, x_i, C_{ij}, c]\,\mathrm{d}r = 0 \tag{13}$$

The radius corresponding to the peak value, c, can take any value between the inner and outer radii, each resulting in one independent equation. Therefore, from every differential equation any number of algebraic equations can be obtained, each corresponding to a specific value of c. After performing the integration for a specific value of c a typical equation can be shown as:

$$q[p, \omega, \rho, x_i, C_{ij}] = 0 \tag{14}$$

Note that Eq. (14) is equivalent to the three equations of motion; however, those are simple algebraic equations. FS expansions of unknown functions transform the derivatives to simple sine and cosine terms, and weighted residual integration removes the r dependence. Although it is an algebraic set of linear equations the solution is not straightforward. In differential equations of motion (6) all terms contain one of $U_r(r)$, $U_t(r)$, $U_f(r)$ or their derivatives. This leads to a form for the above algebraic equations where all terms contain x_i, constituting a system of homogeneous equations. It should be noted that Eqs. (14) must be used to obtain the unknown functions, i.e., $U_r(r)$, $U_t(r)$ and $U_f(r)$. The above mentioned form for the equations implies that more than one solution is available for the unknown functions. Therefore, the general solution should be a linear combination of all solution functions that can be obtained. The general solution should contain combinatorial parameters. The number of combinatorial parameters is the same as the number of individual solutions. These combinatorial parameters are necessary to satisfy the boundary conditions. Satisfaction of six boundary conditions requires six parameters and six equations. Therefore, the necessary and sufficient number of combinatorial parameters is six, and this indicates the existence of six independent solutions.

Substitution of solution functions into the differential equations leads to three equations, each containing all of the FS parameters. In other words, all FS parameters for the three amplitude functions appear in every equation. Because of this coupling, the value of the parameters obtained for FS expansion of $U_r(r)$, $U_t(r)$ and $U_f(r)$ are not independent and a solution must yield all parameters as one set of results. Since the equations are linear and the results must be combined using combinatorial parameters only their relative values are important. Therefore, one of the FS parameters can be assumed to be one. Then the relative values for other FS parameters can be calculated. To avoid repetition in solving the equation sets, the usage of LU factorization is beneficial. Each set of the parameter values defines a set of dependent shapes for the above amplitude functions; these may be called basic shapes. Since the number of equations must be equal to the number of unknowns, a specific number of weight functions are required.

The FS expansion for $U_r(r)$ can be written as Eq. (11), which contains $2m + 1$ parameters or coefficients. With two other expressions for $U_r(r)$ and $U_f(r)$ the number of unknowns increases to $6m + 3$. Eq. (14) can then be written as:

$$\begin{pmatrix} a_{1,1}x_1 & a_{1,2}x_2 & \dots & a_{1,s}x_s & a_{1,s+1}x_{s+1} & \cdot & a_{1,s+6}x_{s+6} \\ a_{2,1}x_1 & a_{2,2}x_2 & \dots & a_{2,s}x_s & a_{2,s+1}x_{s+1} & \cdot & a_{2,s+6}x_{s+6} \\ \cdot & \cdot & \cdots & \cdot & \cdot & \cdot & \cdot \\ \cdot & \cdot & \cdots & \cdot & \cdot & \cdot & \cdot \\ \cdot & \cdot & \cdots & \cdot & \cdot & \cdot & \cdot \\ a_{s,1}x_1 & a_{s,2}x_2 & \dots & a_{s,s}x_s & a_{s,s+1}x_{s+1} & \cdot & a_{s,s+6}x_{s+6} \end{pmatrix} = \begin{pmatrix} 0 \\ 0 \\ \cdot \\ \cdot \\ \cdot \\ 0 \end{pmatrix} \tag{15}$$

where $x_{s+1}, x_{s+2}, \ldots, x_{s+6}$ represent the last sine and cosine terms of FS expansions. Assigning six independent unit vectors to the last six parameters, as shown in Eq. (16),

$$\begin{pmatrix} x^1_{s+1} & x^2_{s+1} & x^3_{s+1} & x^4_{s+1} & x^5_{s+1} & x^6_{s+1} \\ x^1_{s+2} & x^2_{s+2} & x^3_{s+2} & x^4_{s+2} & x^5_{s+2} & x^6_{s+2} \\ x^1_{s+3} & x^2_{s+3} & x^3_{s+3} & x^4_{s+3} & x^5_{s+3} & x^6_{s+3} \\ x^1_{s+4} & x^2_{s+4} & x^3_{s+4} & x^4_{s+4} & x^5_{s+4} & x^6_{s+4} \\ x^1_{s+5} & x^2_{s+5} & x^3_{s+5} & x^4_{s+5} & x^5_{s+5} & x^6_{s+5} \\ x^1_{s+6} & x^2_{s+6} & x^3_{s+6} & x^4_{s+6} & x^5_{s+6} & x^6_{s+6} \end{pmatrix} = \begin{pmatrix} 1 & 0 & 0 & 0 & 0 & 0 \\ 0 & 1 & 0 & 0 & 0 & 0 \\ 0 & 0 & 1 & 0 & 0 & 0 \\ 0 & 0 & 0 & 1 & 0 & 0 \\ 0 & 0 & 0 & 0 & 1 & 0 \\ 0 & 0 & 0 & 0 & 0 & 1 \end{pmatrix} \tag{16}$$

one can obtain six independent solutions. Therefore, the number of equations has to be $s = 6m - 3$. Consequently, the general solution can be obtained as a linear combination of the above solutions.

$$A_1 \begin{pmatrix} x^1_1 \\ x^1_2 \\ \cdot \\ \cdot \\ \cdot \\ x^1_s \end{pmatrix} + A_2 \begin{pmatrix} x^2_1 \\ x^2_2 \\ \cdot \\ \cdot \\ \cdot \\ x^2_s \end{pmatrix} + A_3 \begin{pmatrix} x^3_1 \\ x^3_2 \\ \cdot \\ \cdot \\ \cdot \\ x^3_s \end{pmatrix} + A_4 \begin{pmatrix} x^4_1 \\ x^4_2 \\ \cdot \\ \cdot \\ \cdot \\ x^4_s \end{pmatrix} + A_5 \begin{pmatrix} x^5_1 \\ x^5_2 \\ \cdot \\ \cdot \\ \cdot \\ x^5_s \end{pmatrix} + A_6 \begin{pmatrix} x^6_1 \\ x^6_2 \\ \cdot \\ \cdot \\ \cdot \\ x^6_s \end{pmatrix} \tag{17}$$

The superscript for FS parameters shows the solution set number. Substitution of the obtained FS parameters into stress components on the inner and outer surfaces of the sphere leads to an eigenvalue problem. The determinant of the coefficients of A_i should be zero for any point located on the dispersion curves.

7. Numerical results

In order to check the new formulation, first a number of spherical plate problems with large radius and small thickness are solved. Dispersion curves for such low curvature plates should be similar to the dispersion curves for flat plates. Available numerical results for flat plates matched very well with these results. Additionally, dispersion curves reported for a steel sphere submerged in water are compared with the results obtained using the software prepared for this study. Good agreement between the results ensures the validity of the new formulation technique as well as the computer program. Then a number of dispersion curves are obtained for isotropic and anisotropic spherical plates of different curvatures.

For the isotropic case, aluminum and steel plates are studied. Material properties of aluminum and steel are shown in Figs. 4 and 6, respectively. For the anisotropic case, a fiber reinforced composite material is considered with the mass density, $\rho = 1580$ kg/m^3, and the following constitutive matrix:

$$\begin{pmatrix} \sigma_{\phi\phi} \\ \sigma_{\theta\theta} \\ \sigma_{rr} \\ \sigma_{\theta r} \\ \sigma_{\phi r} \\ \sigma_{\theta\phi} \end{pmatrix} = \begin{pmatrix} 128.2 & 6.9 & 6.9 & 0 & 0 & 0 \\ 6.9 & 14.95 & 7.33 & 0 & 0 & 0 \\ 6.9 & 7.33 & 14.95 & 0 & 0 & 0 \\ 0 & 0 & 0 & 3.81 & 0 & 0 \\ 0 & 0 & 0 & 0 & 6.73 & 0 \\ 0 & 0 & 0 & 0 & 0 & 6.73 \end{pmatrix} \cdot \begin{pmatrix} e_{\phi\phi} \\ e_{\theta\theta} \\ e_{rr} \\ 2e_{\theta r} \\ 2e_{\phi r} \\ 2e_{\theta\phi} \end{pmatrix} \tag{18}$$

Stiffness values are given in GPa.

When the fiber orientation is changed to 45° relative to the wave propagation direction, the constitutive matrix after transformation changes to:

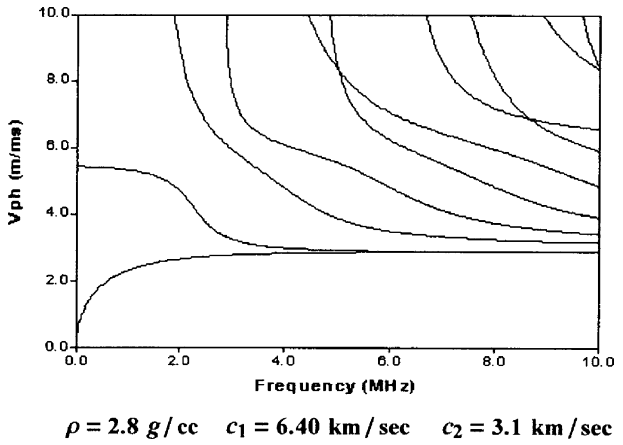

Fig. 4. Dispersion curves for 1 mm thick isotropic flat aluminum plate (Mal and Singh, 1991).

$$\begin{pmatrix} \sigma_{\phi\phi} \\ \sigma_{\theta\theta} \\ \sigma_{rr} \\ \sigma_{\theta r} \\ \sigma_{\phi r} \\ \sigma_{\theta\phi} \end{pmatrix} = \begin{pmatrix} 45.9675 & 32.5075 & 7.115 & 0 & 0 & -28.3125 \\ 32.5075 & 45.9675 & 7.115 & 0 & 0 & -28.3125 \\ 7.115 & 7.115 & 14.95 & 0 & 0 & 0.215 \\ 0 & 0 & 0 & 5.27 & -1.46 & 0 \\ 0 & 0 & 0 & -1.46 & 5.27 & 0 \\ -28.3125 & -28.3125 & 0.215 & 0 & 0 & 32.3375 \end{pmatrix} \cdot \begin{pmatrix} e_{\phi\phi} \\ e_{\theta\theta} \\ e_{rr} \\ 2e_{\theta r} \\ 2e_{\phi r} \\ 2e_{\theta\phi} \end{pmatrix} \tag{19}$$

Similarly, when fibers are going in the 90° direction, relative to the wave propagation direction, then the constitutive matrix takes the following form:

$$\begin{pmatrix} \sigma_{\phi\phi} \\ \sigma_{\theta\theta} \\ \sigma_{rr} \\ \sigma_{\theta r} \\ \sigma_{\phi r} \\ \sigma_{\theta\phi} \end{pmatrix} = \begin{pmatrix} 14.95 & 6.9 & 7.33 & 0 & 0 & 0 \\ 6.9 & 128.2 & 6.9 & 0 & 0 & 0 \\ 7.33 & 6.9 & 14.95 & 0 & 0 & 0 \\ 0 & 0 & 0 & 6.73 & 0 & 0 \\ 0 & 0 & 0 & 0 & 3.81 & 0 \\ 0 & 0 & 0 & 0 & 0 & 6.73 \end{pmatrix} \cdot \begin{pmatrix} e_{\phi\phi} \\ e_{\theta\theta} \\ e_{rr} \\ 2e_{\theta r} \\ 2e_{\phi r} \\ 2e_{\theta\phi} \end{pmatrix} \tag{20}$$

It can be seen that for inclined orientation of fibers the constitutive matrix does not correspond to the transversely isotropic case and requires a more general solution technique. Dispersion curves for a flat aluminum plate are given in Mal and Singh (1991), see Fig. 4. Curves for the same plate thickness and material properties but having a spherical curvature with an outer radius of 100 m are generated by the proposed formulation as shown in Fig. 5a. This figure is generated with $m = 8$ (or 8 terms of the Fourier series expansion, see Eq. (9)). A comparison of Figs. 4 and 5a shows an excellent match between the two. Therefore, one can rely on the new formulation and computed results.

Fig. 5b shows the dispersion curves for an aluminum spherical plate when the outer radius of curvature of the plate is reduced from 100 m in Fig. 5a to 2.5 mm. One can see in these figures that the number of modes increases as the plate curvature increases. Fig. 5c shows the dispersion curves for the wave propagation in the circumferential direction of a cylindrical aluminum plate having a 2.5 mm outer radius of curvature. It was computed following the formulation presented in Towfighi et al. (2002). Note that except for the shape of the plate (for Fig. 5b it is spherical, and for Fig. 5c it is cylindrical) there is no difference between the plates. Both are made of aluminum and have the same thickness and outer radius. Dispersion curves in Fig. 5b and c are almost identical except at low frequencies (below 1 MHz). Some difference is

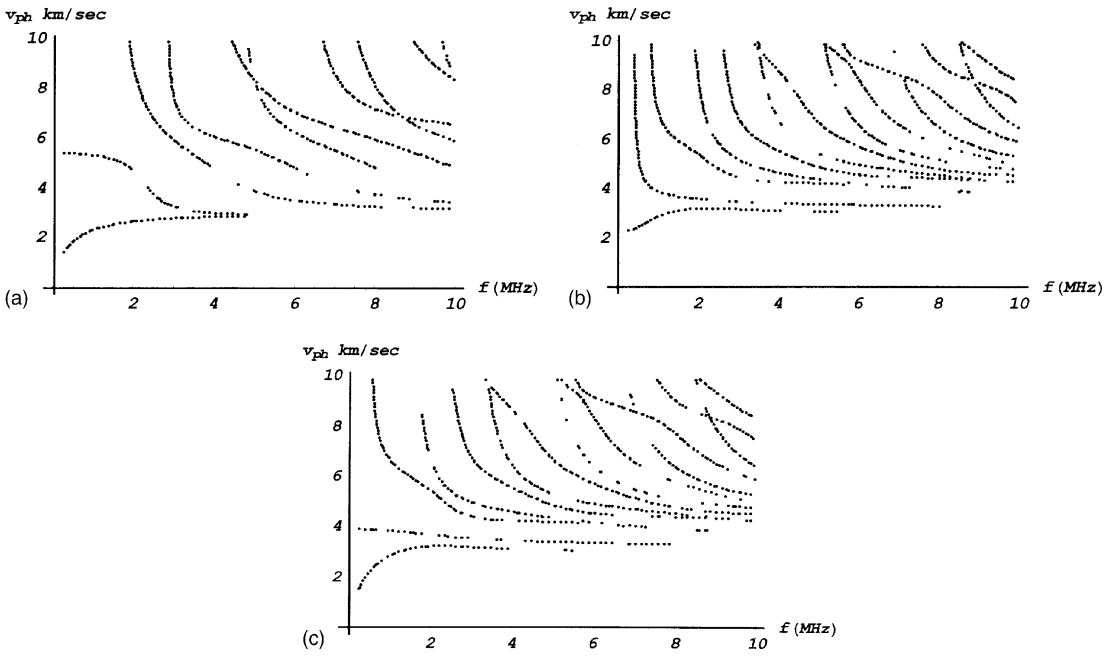

Fig. 5. (a) Dispersion curves generated by the proposed method for a large radius aluminum spherical plate, $m = 8$, plate thickness = 1 mm, sphere outside radius = 100 m. Material properties are given in Fig. 4. (b) Dispersion curves generated by the proposed method for a small radius spherical plate. Aluminum plate thickness = 1 mm. Sphere outside radius = 2.5 mm, $m = 8$, material properties are given in Fig. 4. (c) Same as (b) but for waves propagating in the circumferential direction of a cylindrical curved plate.

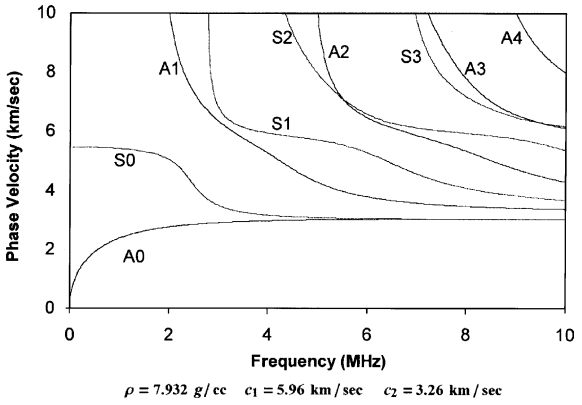

Fig. 6. Dispersion curves for isotropic flat steel plate, plate thickness = 1 mm, material properties are as shown.

expected since for cylindrical plates there is no curvature in the plate geometry in the direction perpendicular to the wave propagation direction while for the spherical plate a curvature in the plate geometry exists in the direction perpendicular to the wave propagation direction. This geometry change does not affect the high frequency, low wavelength waves but the low frequency, long wavelength signals are affected by this change in geometry.

Fig. 6 shows dispersion curves for a flat steel plate. Its material properties are given in the figure. Fig. 7a and b show dispersion curves for the spherical steel plate with the 100 m outer radius (Fig. 7a) and 2.5 mm outer radius (Fig. 7b) with material properties that are the same as the flat steel plate. Figs. 6 and 7a match very well. Fig. 7a is computed with $m = 8$, like Fig. 5a. Fig. 7b shows more curves than Fig. 7a—this observation is similar to our findings in Fig. 5a and b. Fig. 7c shows dispersion curves for cylindrical curved plate for waves propagating in the circumferential direction. Like Fig. 5b and c, differences between Fig. 7b and c are observed only at low frequencies.

Fig. 8a shows dispersion curves obtained by Gaunaurd and Werby (1991a) for a steel sphere submerged in water. Using the same steel properties and curvature (thickness to outer radius ratio = 0.05), dispersion curves for a spherical plate segment are obtained by the current method, and presented in Fig. 8b. Small differences between the two sets of dispersion curves are attributed to the fact that in one case (Fig. 8a) a complete sphere is submerged in water, and for the other case (Fig. 8b) the spherical plate segment is placed in a vacuum, not in water.

The dispersion curves for anisotropic materials are studied next. Dispersion curves for anisotropic flat plates are available in the literature (Karim et al., 1990; Rose, 1999). In this paper our results are compared with those given in Rose (1999). Fig. 9 shows dispersion curves for a flat anisotropic plate when fibers are oriented parallel to the wave propagation direction. Fig. 10a shows dispersion curves for the same anisotropic material when formed as a spherical plate with 100 m outer radius. Like other curves this is also generated with $m = 8$, and show good matching with Fig. 9. Fig. 10b and c show the effect of the higher curvature on the dispersion curves. These two plots are generated for the same material properties but different plate geometries—for Fig. 10b the outer radius of the sphere is 5 mm and for Fig. 10c it is 2.5 mm. Like the isotropic case, the number of modes increases as the plate curvature increases. Dispersion curves

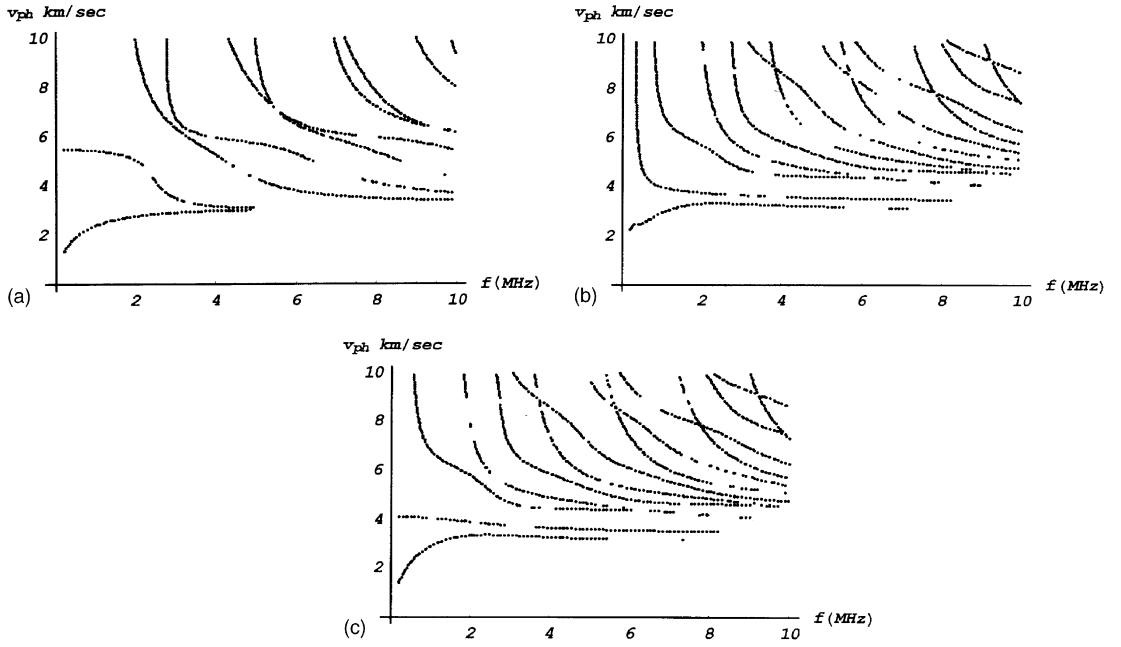

Fig. 7. (a) Dispersion curves generated by the proposed method for a large radius spherical steel plate, $m = 7$, plate thickness = 1 mm, sphere outside radius = 100 m. Material properties are given in Fig. 6. (b) Dispersion curves generated by the proposed method for a small radius spherical plate. Steel plate thickness = 1 mm. Sphere outside radius = 2.5 mm, $m = 8$, material properties are given in Fig. 6. (c) Same as Fig. 7b but for waves propagating in the circumferential direction of a cylindrical curved plate.

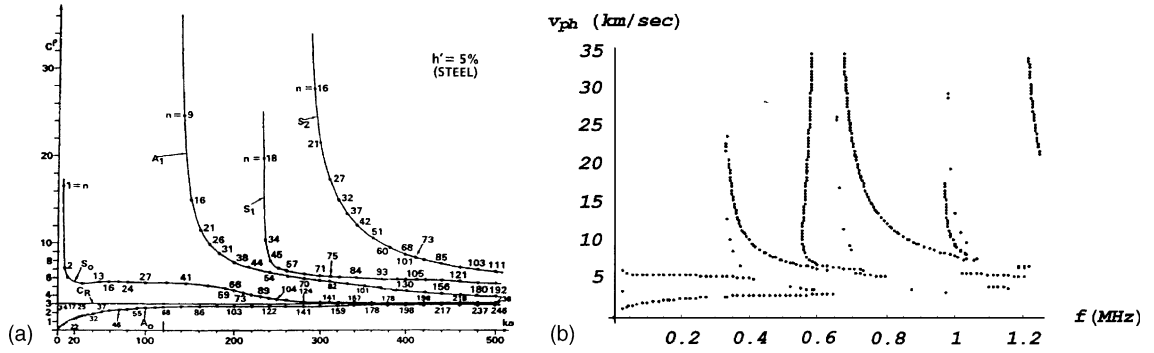

Fig. 8. (a) Dispersion curves for a steel sphere, submerged in water, after Gaunaurd and Werby (1991a). Wall thickness to outer radius is 0.05. Density, P-wave speed and S-wave speed for steel are 7.7 gm/cc, 5.95 km/s and 3.24 km/s, respectively. Those values for water are 1 gm/cc, 1.4825 km/s and zero. Horizontal axis shows the non-dimensional frequency, $k_m = (\omega/c_1)a$. For 95 mm inner radius sphere, non-dimensional frequency = 500 corresponds to 1.242 MHz frequency, for this steel plate. (b) Dispersion curves for a spherical steel plate segment in vacuum. Steel properties are identical to those given in (a). Wall thickness to outer radius is 0.05.

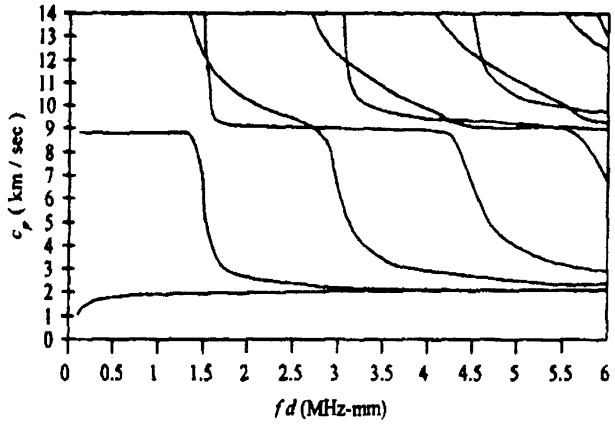

Fig. 9. Dispersion curves for a unidirectional composite plate for waves propagating in the fiber direction (x-axis direction, 0°). Material properties are given in Eq. (18), $\rho = 1580$ kg/m^3 (Rose, 1999).

for the circumferential direction wave propagation in a cylindrical plate with 2.5 mm outer radius are shown in Fig. 10d. Note that except at low frequencies (less than 1.5 MHz) the dispersion curves in Fig. 10c and d are identical.

Fig. 11 shows dispersion curves for an aniostropic flat plate when waves propagate perpendicular to the fiber direction. Fig. 12a, b and c show dispersion curves for spherical plates of outer radius 100 m, 5 mm and 2.5 mm, respectively, for fiber and wave propagation directions perpendicular to each other. Fig. 12a matches very well with Fig. 11. Fig. 12d shows the dispersion curves for the circumferential direction wave propagation in a cylinder of 2.5 mm outer radius when the fibers run along the axial direction. A comparison between Fig. 12c and d show difference in the dispersion curves only in the low frequency range 0–1 MHz.

Similar computations have been carried out for the 45° fiber direction relative to the wave propagation direction. Flat plate results from the literature are shown in Fig. 13a and b. Spherical plate results for the outer radius equal to 100 m, 5 mm and 2.5 mm are shown in Fig. 14a, b and c respectively. Like the

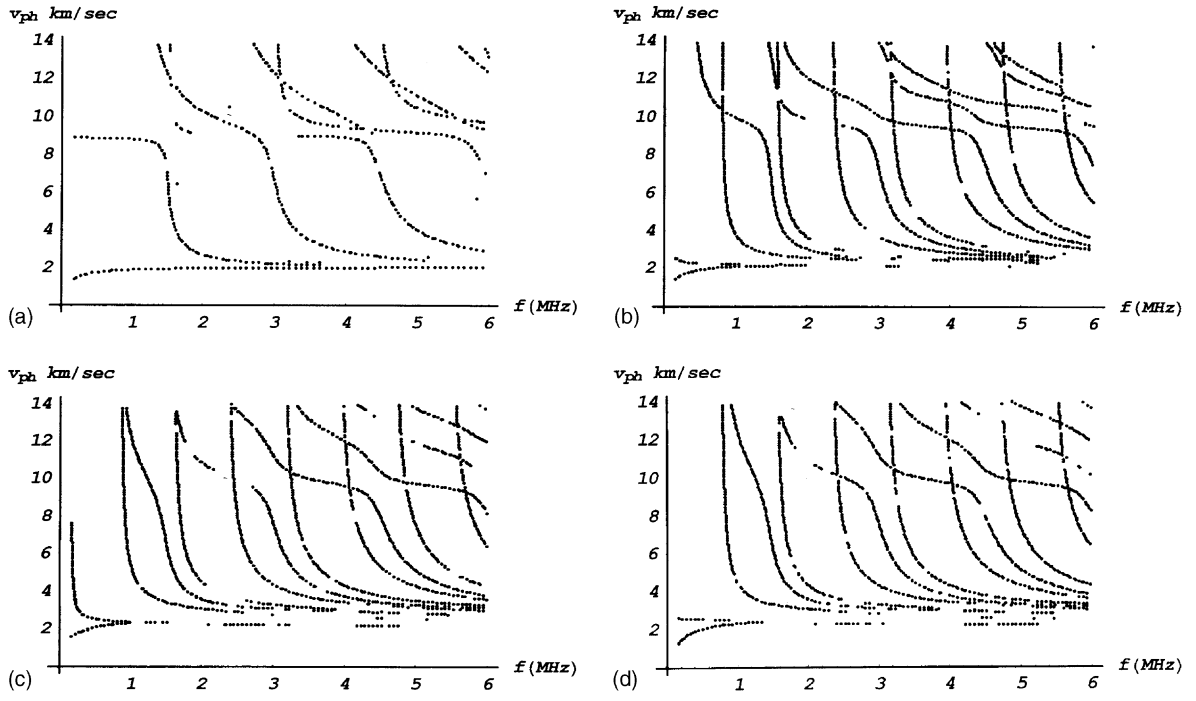

Fig. 10. (a) Dispersion curves generated by the proposed method for a large radius spherical plate, material properties are same as those used in Fig. 9, $m = 8$, plate thickness = 1 mm, outer radius of the curved plate = 100 m. (b) Dispersion curves generated by the proposed method for same material properties as those used in Fig. 9, plate thickness = 1 mm, outer radius of the curved plate = 5 mm, $m = 8$. (c) Dispersion curves generated by the proposed method for same material properties as those used in Fig. 9, plate thickness = 1 mm, outer radius of the curved plate = 5 mm, $m = 15$. (d) Same as (c) but for waves propagating in the circumferential direction of a cylindrical curved plate.

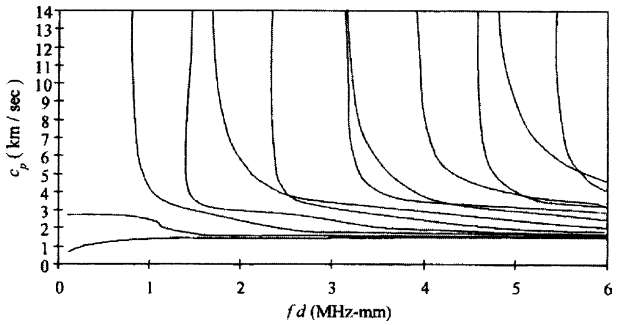

Fig. 11. Dispersion curves of unidirectional composite plate for waves propagating perpendicular to the fiber direction (x-axis direction, 90°). Material properties are given in Eq. (20). Plate thickness = 1 mm, $\rho = 1580$ kg/m^3 (Rose, 1999).

previous cases Fig. 14a matches exactly with Fig. 13 when Fig. 13a and b are superimposed. Dispersion curves gradually change from Fig. 14a–c. Dispersion curves of Fig. 14d are generated when the spherical plate for Fig. 14c is changed to a cylindrical plate, with waves propagating in the circumferential direction and the fibers are oriented at 45°. Dispersion curves of Fig. 14c and d are almost identical for frequencies greater than 3 MHz.

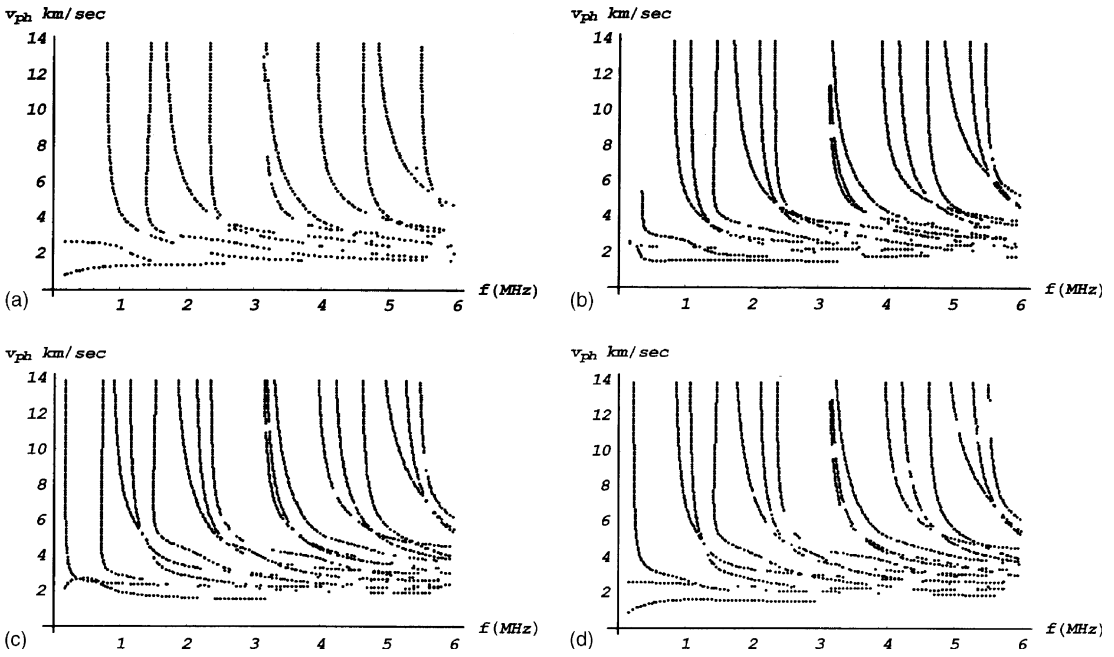

Fig. 12. (a) Computed dispersion curves for an anisotropic large radius spherical plate, when fiber and wave propagation directions are perpendicular to each other. Material properties are given in Eq. (20). Plate thickness = 1 mm. Outer radius of the spherical curved plate = 100 m, $m = 8$. (b) Computed dispersion curves for an anisotropic small radius spherical plate, when fiber and wave propagation directions are perpendicular to each other. Material properties are given in Eq. (20). Plate thickness = 1 mm. Outer radius of the spherical plate = 5 mm, $m = 8$. (c) Computed dispersion curves for an anisotropic small radius spherical plate, when fiber and wave propagation directions are perpendicular to each other. Material properties are given in Eq. (20). Plate thickness = 1 mm. Outer radius of the spherical plate = 2.5 mm, $m = 8$. (d) Same as (c) but for a cylindrical curved plate when waves are propagating in the circumferential direction.

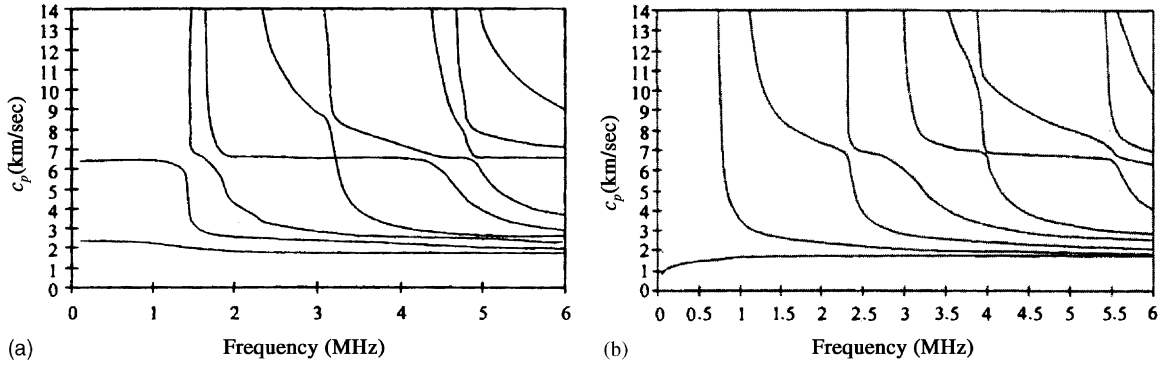

Fig. 13. (a) Dispersion curves for symmetric modes for a unidirectional composite plate for waves propagating in 45° to the fiber direction. Plate thickness = 1 mm and $\rho = 1580$ kg/m^3 (Rose, 1999). (b) Dispersion curves for antisymmetric modes for a unidirectional composite plate for waves propagating in 45° to the fiber direction. Plate thickness = 1 mm and $\rho = 1580$ kg/m^3 (Rose, 1999).

It is interesting to note that for high curvature (outer radius to thickness ratio = 2.5) the differences in the dispersion curves, generated by isotropic spherical and cylindrical plates, disappear beyond 1 MHz. For anisotropic plate however, this frequency depends on the fiber direction. For 45° fiber orientation, up to 3

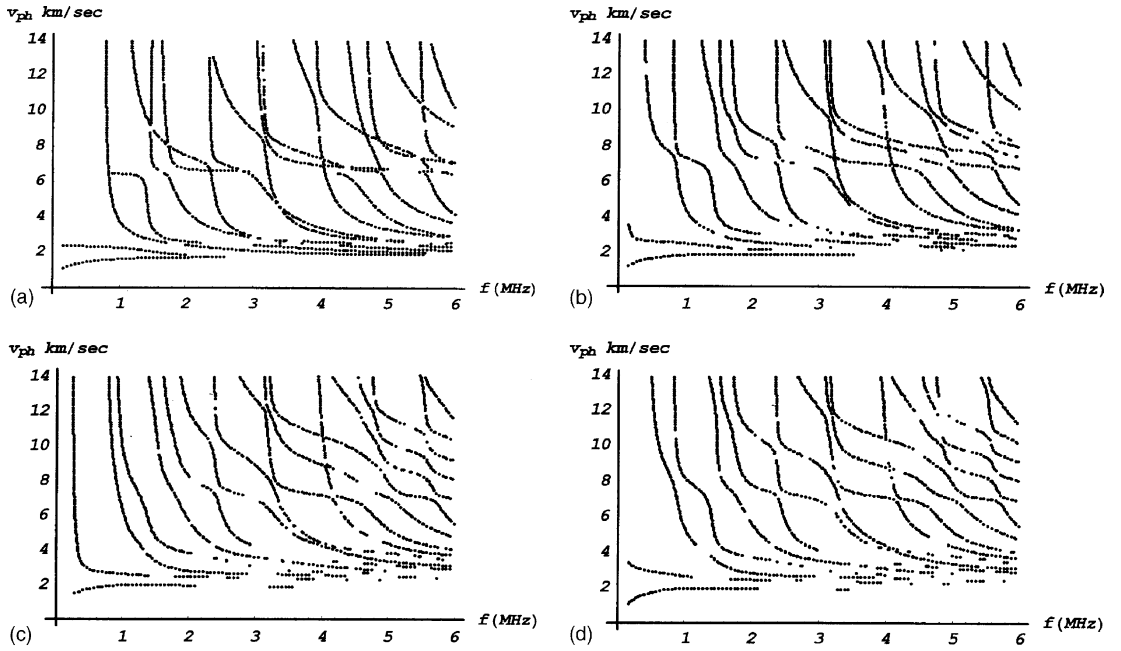

Fig. 14. (a) Computed dispersion curves for an anisotropic large radius spherical plate for waves propagating in 45° to the fiber direction. Material properties are given in Eq. (19). Plate thickness = 1 mm. Outer radius of the spherical plate = 100 m, $m = 8$. (b) Computed dispersion curves for an anisotropic small radius spherical plate for waves propagating in 45° to the fiber direction. Material properties are given in Eq. (19). Plate thickness = 1 mm. Sphere outer radius = 5 mm, $m = 8$. (c) Computed dispersion curves for an anisotropic small radius spherical plate for waves propagating in 45° to the fiber direction. Material properties are given in Eq. (19). Plate thickness = 1 mm. Sphere outer radius = 2.5 mm, $m = 15$. (d) Same as (c) but for a cylindrical curved plate when waves propagate in the circumferential direction.

MHz frequency, differences between the dispersion curves generated by the cylindrical and spherical curved plates are noticeable.

8. Conclusion

The elastic wave propagation problem in spherical curved plates is solved here for both isotropic and anisotropic plate materials. For the anisotropic plate modeling unidirectional fiber reinforced composite plates are considered with fibers running parallel, perpendicular, and at an angle of 45°, relative to the wave propagation direction. Dispersion curves generated by spherical and cylindrical plates are identical at higher frequencies. The frequency beyond which these two sets of dispersion curves are identical depends on the fiber orientation direction. Among the three cases studied here (0°, 45° and 90° orientations of fibers) it is found that the difference in the dispersion curves generated by cylindrical and spherical plates is maximum for the 45° orientation of fibers.

Acknowledgement

This research was partially supported from the National Science Foundation grant CMS-9901221.

References

Armenkas, A.E., Reitz, E.S., 1973. Propagation of harmonic waves in orthotropic, circular cylindrical shell. ASME Journal of Applied Mechanics, 168–174.

Brekhovskikh, L.M., 1968. Surface waves confined to the curvature of the boundary in solid. Soviet Physics—Acoustics 13, 462–472.

Buldyrev, V.S., Lanin, A.I., 1966. Investigation of the interference wave field on the surface of an elastic sphere. In: Collection: Numerical Methods of Solving Problems in Mathematical Physics. Nauka, Moscow. pp. 131–143 (in Russian).

Gaunaurd, G.C., Werby, M.F., 1991a. Similarities between various Lamb waves in submerged spherical shells, and Rayleigh waves in elastic spheres and flat half-spaces. Journal of the Acoustical Society of America 89, 2731–2739.

Gaunaurd, G.C., Werby, M.F., 1991b. Sound scattering by resonantly excited, fluid loaded, elastic spherical shells. Journal of the Acoustical Society of America 90, 2536–2550.

Gazis, D.C., 1959a. Three-dimensional investigation of the propagation of waves in hollow circular cylinders. I. Analytical foundation. Journal of the Acoustical Society of America 31 (5).

Gazis, D.C., 1959b. Three-dimensional investigation of the propagation of waves in hollow circular cylinders. II. Numerical results. Journal of the Acoustical Society of America 31 (5).

Grace, O.D., Goodman, R.R., 1966. Circumferential waves on solid cylinders. Journal of the Acoustical Society of America 39, 173–174.

Junger, M.C., Feit, D., 1986. Sound, Structures, and Their Interactions, second ed. MIT, Cambridge, MA (Chapter 7).

Kargl, S.G., Marston, P.L., 1990. Ray synthesis of lamb wave contributions to the total scattering cross section for an elastic spherical shell. Journal of the Acoustical Society of America 88, 1103–1113.

Karim, M.R., Mal, A.K., Bar-Cohen, Y., 1990. Inversion of leaky lamb wave data by simplex algorithm. Journal of the Acoustical Society of America 88, 482–491.

Lanin, A.I., 1964. Interference wave field near the surface of an inhomogeneous elastic sphere. In: Third All-Union Symposium on Wave Diffraction. Nauka, Moscow, pp. 108–109. Abstract of papers (in Russian).

Liu, G., Qu, J., 1998a. Guided circumferential waves in a circular annulus. ASME Journal of Applied Mechanics 65, 424–430.

Liu, G., Qu, J., 1998b. Transient wave propagation in a circular annulus subjected to impulse excitation on its outer surface. Journal of the Acoustical Society of America 103, 1210–1220.

Mal, A.K., Singh, S.J., 1991. Deformation of Elastic Solids. Prentice-Hall, Englewood Cliffs, New Jersey. p. 313.

Qu, J., Berthelot, Y., Li, Z., 1996. Dispersion of guided circumferential waves in a circular annulus. In: Thompson, D.O., Chimenti, D.E. (Eds.), Review of Progress in Quantitative Nondestructive Evaluation, vol. 15. Plenum, New York, pp. 169–176.

Rose, J.L., 1999. Ultrasonic Waves in Solid Media. Cambridge University Press, Cambridge, UK. pp. 264–271.

Shah, A.H., Ramakrishnan, C.V., Datta, S.K., 1969. Three-dimensional shell-theory analysis of elastic waves in a hollow sphere. ASME Journal of Applied Mechanics 36, 431–439.

Towfighi, S., 2001. Elastic wave propagation in circumferential direction in anisotropic pipes, Ph.D. Dissertation, 2001, The University of Arizona, Tucson, AZ.

Towfighi, S., Kundu, T., Ehsani, M., 2002. Elastic wave propagation in circumferential direction in anisotropic cylindrical curved plates. ASME Journal of Applied Mechanics 69, 283–291.

Überal, H., 2001. Acoustics of shells. Acoustical Physics 47, 115–139.

Valle, C., Qu, J., Jacobs, L.J., 1999. Guided circumferential waves in layered cylinders. International Journal of Engineering Science 37, 1369–1387.

Viktorov, I.A., 1958. Rayleigh-type waves on a cylindrical surface. Soviet Physics—Acoustics 4, 131–136.